CHEMISTRY OF MATERIALS
Cite This: Chem. Mater. 2019, 31, 6163−6173
Article
pubs.acs.org/cm

Terpolymer Strategy toward High-Efficiency Polymer Solar Cells: Integrating Symmetric Benzodithiophene and Asymmetrical Thieno[2,3-*f*]benzofuran Segments

Xunchang Wang,[†,‡] Keke Dou,[§] Bilal Shahid,[†,‡] Zhilin Liu,[†] Yonghai Li,[*,†] Mingliang Sun,[§] Nan Zheng,[*,∥] Xichang Bao,[*,†] and Renqiang Yang[*,†]

[†]CAS Key Laboratory of Bio-based Materials, Qingdao Institute of Bioenergy and Bioprocess Technology, Chinese Academy of Sciences, Qingdao 266101, China

[‡]Center of Materials Science and Optoelectronics Engineering, University of Chinese Academy of Sciences, Beijing 100049, China

[§]Institute of Material Science and Engineering, Ocean University of China, Qingdao 266100, China

[∥]Institute of Polymer Optoelectronic Materials and Devices, State Key Laboratory of Luminescent Materials and Devices, South China University of Technology, Guangzhou 510640, China

Supporting Information

ABSTRACT: While a large number of terpolymers have been developed for polymer solar cells, very few studies have directly focused on the rational selection of the third component to balance the miscibility and crystallinity for forming the desired morphology, and universal terpolymer strategies for preparing different donor/acceptor systems are lacking. Herein, we employ a new strategy involving the integration of benzodithiophene (BDT) and thieno[2,3-*f*]benzofuran (TBF) segments to construct a series of terpolymer donors, and a profound influence on the crystallinity and miscibility of the blend films as well as on the ultimate device performance is observed. Incorporating highly crystalline TBF segments into a low-crystalline BDT-based alternating copolymer can not only increase the order of the microstructure, conserve the favorable face-on orientation, and promote the formation of proper phase-separation features but also generate high exciton dissociation and suppress charge recombination. This strategy was successfully applied in the reported J52 system and provided a remarkable 2-fold boost in performance. Finally, competitive power conversion efficiencies of 11.9, 12.4, and 12.2% accompanied by high fill factors of 73, 71, and 76% were recorded for TBFCl50-FTAZ/ITIC-, TBFCl50-BDD/ITIC-, and TBFCl50-BDD/IDIC-C4Ph-based devices, respectively, via the above terpolymer strategy. Thus, our discovery provides a promising and innovative method for finely controlling the microstructure of heterojunctions for designing high-performance terpolymers.

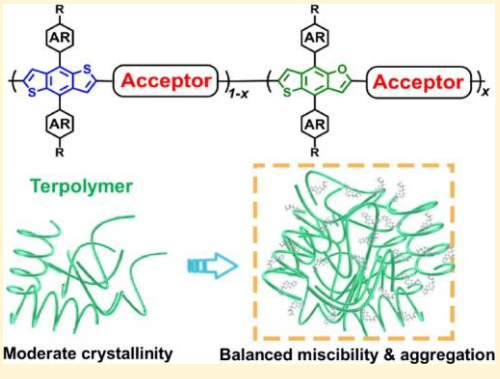

INTRODUCTION

Solution-processed bulk-heterojunction (BHJ) polymer solar cells (PSCs), which are considered as a flexible, transparent, environmentally friendly, low-cost, and printable solar technology,[1−6] have attracted enormous attention in recent years, and the power conversion efficiencies (PCEs) of single-junction PSCs have recently exceeded 15%.[7−10] The rapid advances in PCEs are mainly attributed to important developments in novel electron-donor and electron-acceptor materials, as well as the discovery of new processing technologies and device architectures.[11−31] For the design of novel donor materials, an alternating donor−acceptor (D−A) copolymer strategy has been recognized as a particularly important approach for tuning the energy levels, optical properties, charge carrier mobility, and crystallinity of materials.[32−37] However, in some cases, due to the fixed structures of alternating D−A polymers, these properties as well as the miscibility with acceptors could not reach the optimum required for state-of-the-art solar cells.

Another method for constructing efficient donor polymers is the terpolymer strategy, which involves polymers with three distinct moieties in their chains.[29,38] With the embedding of a third compound into the D−A alternating copolymer backbone to form a terpolymer, the optical absorption, electrical properties, crystallinity, and charge transport behaviors can be synergistically influenced.[39−51] Reducing the regularity of the polymers by random polymerization can improve solubility, leading to better solution processing.[41,52−54] In addition, adjusting the proportion of each component in the terpolymers should be carefully considered, as the proportions could play a

Received: May 18, 2019
Revised: July 25, 2019
Published: July 25, 2019

DOI: 10.1021/acs.chemmater.9b01957
Chem. Mater. 2019, 31, 6163−6173

Scheme 1. Terpolymer Strategy Applied in the J52 System

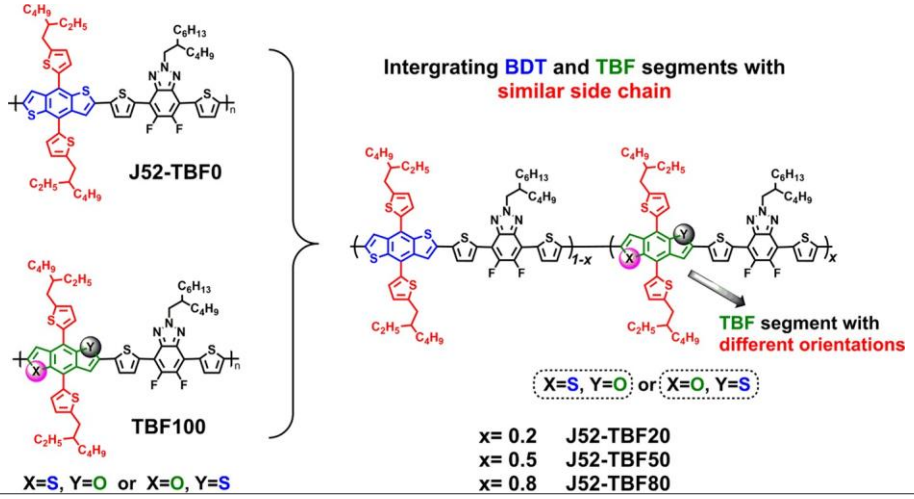

decisive role in determining the final performance.[55] Unfortunately, as most approaches today have involved the use of different sized and shaped monomers, terpolymer architectures are usually limited to polymer backbones with irregular sequences, which complicate the achievement of ordered molecular stacking and appropriate phase-separation properties, limiting the practical potential of the random terpolymer strategy. Moreover, the great differences in intrinsic molecular structures can even exacerbate this problem. Thus, few PSCs based on random terpolymers with PCEs surpassing those of the state-of-the-art PSCs with respective alternating copolymers have been reported.[39,40,43] Accordingly, to achieve the anticipated improvements in the terpolymer-based device, one of the key challenges associated with terpolymers lies in the rational selection of the third component to reduce the structural differences and finely tune the BHJ morphological properties. Here, we assume that the building block size and side chains of the third component are similar to those of the D or A moieties and that the third segment can modulate the aggregation in the polymers. After the third segment was incorporated into the D−A polymer backbone, the regioregularity of the polymer was not dramatically perturbed, and the degree of crystallinity, ordered phase separation, and π−π stacking orientations of the terpolymers could be maintained. Additionally, a balance between crystallinity and miscibility in the BHJ blend films could be achieved with the target terpolymers by carefully adjusting the ratio of the three components.

To confirm the above assumption, we proposed the terpolymer strategy by simultaneously employing the classical benzodithiophene (BDT) and infrequently used thieno[2,3-*f*]benzofuran (TBF) as electron-rich units to construct BDT-A-TBF-A terpolymers.[56,57] For TBF, a structure asymmetric derivative of BDT with one of the two sulfur atoms replaced by oxygen atom generates higher crystallinity and denser intermolecular π−π stacking in the resulting D−A polymers, comparable to those of the BDT counterparts. Because the structures of BDT and TBF are almost identical and they can both be readily modified by same side chains, we believe that the design strategy for terpolymers involved with BDT and TBF components could be highly promising and synergistic advantages of these three moieties can be expected.

The BDT-A-TBF-A terpolymer strategy was first applied in polymer J52, whose performance was relatively poor compared with classical wide-band-gap conjugated polymers J51, J61, and J71 when blended with ITIC.[58−62] We found that random polymerization in the presence of TBF effectively enhanced the aggregation of the D−A copolymer J52 and provided a new terpolymer with a highly ordered packing structure and moderate miscibility with ITIC in BHJ films. As a result, the terpolymer J52-TBF50, which contained 50% TBF units, provided a remarkable 2-fold boost in performance. To further verify the universality of this design strategy, we designed a new TBF unit modified by chlorinated side chains to decrease the highest occupied molecular orbital (HOMO) levels of the terpolymers. Two new BDT-A-TBF-A terpolymers, named TBFCl50-FTAZ and TBFCl50-BDD, were then synthesized, and competitive PCEs of 11.94, 12.46, and 12.29% accompanied by high fill factors (FFs) of 73.81, 71.33, and 76.63% were recorded for TBFCl50-FTAZ/ITIC-, TBFCl50-BDD/ITIC-, and TBFCl50-BDD/IDIC-C4Ph-based devices, respectively.[63] Furthermore, the excellent processability of the terpolymers enabled only slight deviations from the optimal BHJ nanomorphology, and a device area of 0.8 cm^2 and PCEs over 10% were achieved. These results demonstrated the great potential of the BDT-A-TBF-A terpolymer strategy to enhance the BHJ microstructures of terpolymer PSCs, improving their performance, large-scale producibility, and industrial viability.

RESULTS AND DISCUSSION

Material Synthesis and Characterization. As shown in Scheme 1, the two D−A copolymers, J52-TBF0 and TBF100, and three random BDT-A-TBF-A terpolymers, J52-TBF20, J52-TBF50, and J52-TBF80, were prepared with different feed molar ratios using a palladium-catalyzed cross-coupling condensation polymerization. The details of the polymerization procedures are described in the Supporting Information (Scheme S1). All of the terpolymers possess different backbone structures, symmetric BDT, and asymmetric TBF units but have identical side chains. High-temperature gel permeation chromatography was used to determine the number-average molecular weights (M_n values) of the polymers, and 1,3,5-trichlorobenzene was used as the eluent. The number-average M_n values and polydispersity index (PDIs) for the five polymers are summarized in Table S1

DOI: 10.1021/acs.chemmater.9b01957
Chem. Mater. 2019, 31, 6163−6173

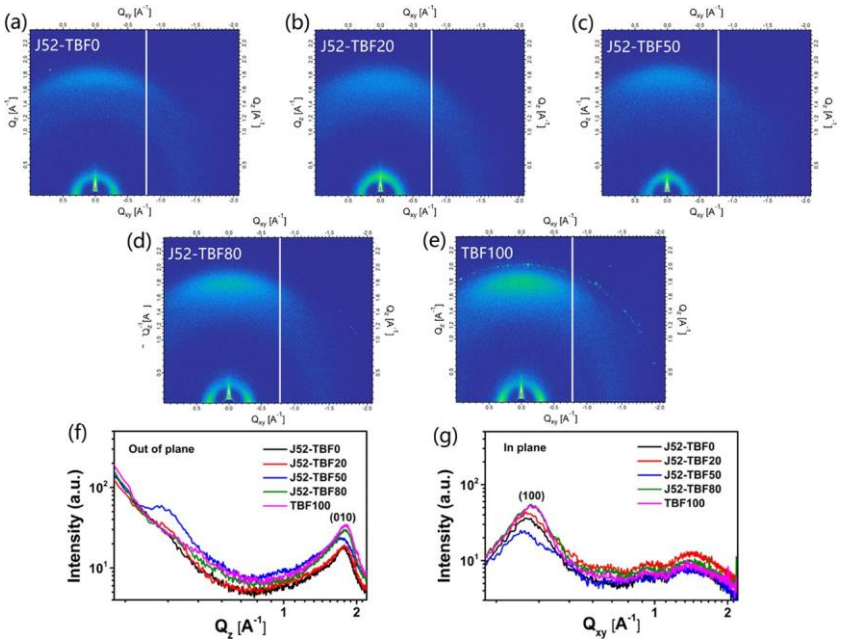

Figure 1. (a−e) Two-dimensional-GIWAXS patterns of the neat polymer films. (f, g) Corresponding out-of-plane and in-plane GIWAXS line-cut profiles, respectively.

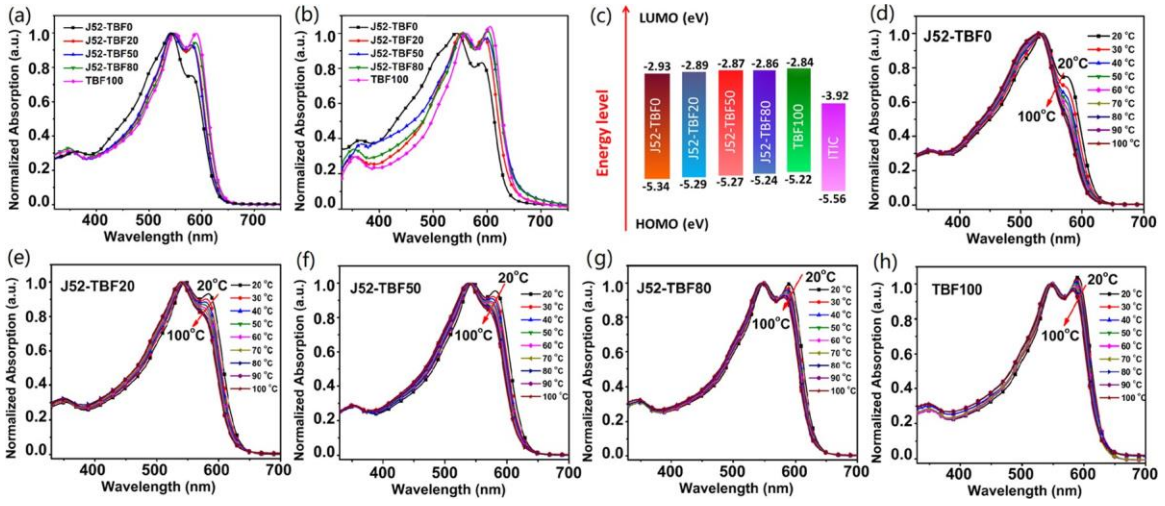

Figure 2. UV−vis absorption spectra of the polymers (a) in solution and (b) in the solid state. (c) Energy-level diagrams of the corresponding polymer donors and ITIC acceptor. The temperature-dependent UV−vis absorption spectra of (d) J52-TBF0, (e) J52-TBF20, (f) J52-TBF50, (g) J52-TBF80, and (h) TBF100 in dilute solutions in $CHCl_3$.

(Figure S1). The polymers exhibited excellent solubility in common organic solvents such as chloroform, toluene, and chlorobenzene (CB) at room temperature. The thermogravimetric analysis (TGA) curves showed that the decomposition temperatures (T_d, 5% weight loss) of the polymers were more than 350 °C, indicating that their thermal stability was sufficient for device processing (Figure S2).

Intermolecular Packing Measurement of the Pure Polymer Films. Grazing-incidence wide-angle X-ray scattering (GIWAXS) analysis was performed to investigate the molecular orientations of the polymers and their crystalline properties. Figure 1a−e shows the two-dimensional (2D)-GIWAXS patterns of the neat polymers, and the corresponding in-plane and out-of-plane (OOP) scattering profiles are displayed in Figure 1f,g, respectively. Notably, all of the terpolymers showed predominantly face-on orientations, with a sharp (010) π−π stacking peak only in the out-of-plane direction, indicating that the favorable face-on orientation of the terpolymers is maintained upon incorporation of TBF segments into the material. Moreover, the BDT-A-TBF-A terpolymer with the same side chains can tolerate the randomly arranged units, resulting in similar ordered lamellar packing. In addition, the neat J52 film showed the lowest crystallinity, and the intensity of its (010) peak gradually increased with increasing TBF content in the polymer backbone, suggesting that the order can be enhanced by increasing the content of TBF units. However, as for the neat TBF100 film, the high crystallinity with extremely ordered packing may negatively impact the miscibility of the blend film.[64,65] The above analysis indicates that incorporating TBF units into BDT-based alternating copolymers increases the polymer crystallinity while maintaining the favorable face-on

DOI: 10.1021/acs.chemmater.9b01957
Chem. Mater. 2019, 31, 6163−6173

orientation, indicating that this is a suitable method for controlling the microstructures of polymer films.

Optical and Electrochemical Properties. The UV−vis absorption spectra of the polymers as dilute chloroform solutions and thin solid films are presented in Figure 2a,b, respectively. Compared to J52, the other four polymers showed prominent shoulder peaks at approximately 600 nm both in solution and solid films, implying that more effective aggregation and better interchain packing occurred when TBF units were incorporated into the J52 backbone. In the solid state, the polymers exhibited slightly red-shifted absorption onsets with respect to those in their solution states, which indicated that increased intermolecular stacking occurred in the solid state. As seen in Table 1, there is a relatively little variation in optical band gaps. Temperature-dependent solution absorption (TDA) measurements were also performed starting from room temperature to 100 °C to further investigate the aggregation behaviors of the polymers (Figure 2d−h).

Table 1. Summary of the Optical Properties of Polymers

polymers	λ_{max}^{sol} (nm)	λ_{max}^{film} (nm)	λ_{edge} (nm)	E_g^{opt}[a] (eV)	HOMO[b] (eV)	LUMO[b] (eV)
J52-TBF0	530	536	639	1.94	−5.34	−2.93
J52-TBF20	532	542	646	1.92	−5.29	−2.89
J52-TBF50	533	543	649	1.91	−5.27	−2.87
J52-TBF80	533	544	649	1.91	−5.24	−2.86
TBF100	533	548	650	1.91	−5.22	−2.84

[a]Calculated from the empirical formula: $E_g^{opt} = 1240/\lambda_{edge}$. [b]Obtained from the cyclic voltammetry (CV) method.

Interestingly, although no obvious thermochromic shifts were observed for any of the polymers, the degrees of aggregation were completely different. When the temperature was increased to 50 °C, the aggregation of J52 was almost completely disrupted. With increasing proportions of TBF units, the polymer aggregation increased. In particular, TBF100, with no BDT, exhibited a distinct and sharp shoulder in the long-wavelength region even when the temperature was increased to 100 °C. The TDA results indicated that the incorporation of TBF into BDT-based D−A polymers with same side chains can strongly increase the aggregation and intermolecular packing, even though the target terpolymer backbone is random. Optimizing the content of TBF units in the BDT-A-TBF-A terpolymer is critical to controlling the aggregation and forming active layers with the desired microstructures.

Electrochemical cyclic voltammetry (CV) measurements were utilized to estimate the energy levels of the polymers.[66] Polymer films were deposited on glassy carbon working electrodes and measured in acetonitrile with ferrocene/ferrocenium (Fc/Fc^+) as an internal standard. The energy level of Fc/Fc^+ was assigned an absolute energy of −4.8 eV versus the vacuum level. The oxidation and reduction onset potentials of all of the polymers were estimated in Figure S3, and the HOMO and lowest unoccupied molecular orbital (LUMO) energy levels were calculated according to the equations $E_{(HOMO/LUMO)} = -(E_{ox/red} + 4.35)$ (eV), which are summarized in Table 1. Increasing the TBF content in the polymer backbone from 0 to 100% increased slightly both the HOMO and LUMO levels. Figure 2c shows the energy-level diagrams of the polymers and ITIC for a clear comparison. As the HOMO levels of these terpolymers are far from that of ITIC, there may be great opportunities for decreasing the energy levels, enhancing the open-circuit voltage (V_{oc}) values.

Photovoltaic Properties and Charge Generation, Transport, and Recombination Behaviors of Solar Cells. Solution-processed BHJ solar cells were fabricated to evaluate the photovoltaic performance of the polymers with a conventional device architecture of indium-tin oxide (ITO)/poly(3,4-ethylenedioxythiophene)/poly(styrenesulfonate) (PEDOT:PSS)/active layer/perylenediimide functionalized with amino *N*-oxide (PDINO)/Al. The optimized D/A weight ratios used for the spin-coating solutions were 1:1. The active layers were prepared by spin-coating blend solution with a total blend concentration of 20 mg mL^{-1} in CB, and the optimized thickness was ~120 nm. The devices were further optimized by combining CB solvent vapor annealing (SVA) and thermal annealing (TA) at 140 °C. The annealed devices showed improved device performances with the increased J_{sc} and FF as well as a slightly decreased V_{oc} value when compared with the as-cast devices (Table S2). The current density−voltage ($J-V$)

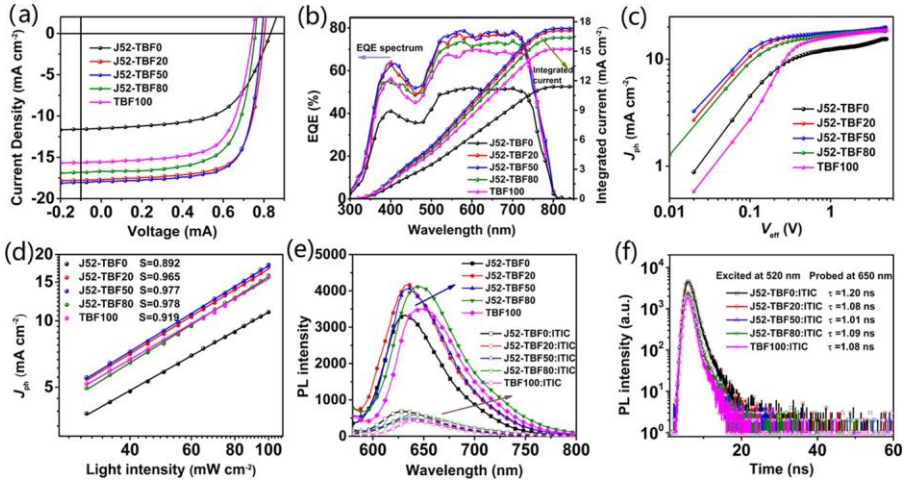

Figure 3. (a) $J-V$ characteristics of the optimized PSCs based on the polymers and ITIC. (b) EQE curves and integrated J_{sc} of the corresponding PSCs. (c) J_{ph} versus V_{eff} curves of the optimized BHJ devices. (d) $J_{ph}-P_{light}$ curves of the optimized devices. (e) Photoluminescence (PL) spectra of the pure polymers and corresponding blend films. (f) Transient PL (TPL) spectra of the five target blend films probed at 650 nm.

DOI: 10.1021/acs.chemmater.9b01957
Chem. Mater. 2019, 31, 6163−6173

curves of the PSC devices under the optimal conditions with active areas of 0.1 cm^2 are shown in Figure 3a, and the corresponding data are summarized in Table 2. Notably, increasing the content of TBF units from 0 to 50% sharply increased both J_{sc} and FF. When the content of the TBF units in the terpolymer exceeds 50%, the J_{sc} and FF values gradually decreased. The best performance was obtained from the J52-TBF50-based device, which shows a high PCE of 10.32% and provides a remarkable 2-fold boost for the J52-based device, indicating that the BDT-A-TBF-A strategy can strongly improve the photovoltaic performance. As shown in Figure 3b, the external quantum efficiency (EQE) curves of all of the devices reflected the same trend as that of the UV−vis absorption spectra of the corresponding polymers ranging from 300 to 800 nm. Notably, the integrated photocurrents from the EQE tests were in good agreement with those obtained from the $J-V$ curves, and they showed deviations of less than 5%.

To understand the charge transport evolution induced by the incorporation of TBF units, we first investigated the charge mobility of all of the polymer/ITIC blends using the space-charge-limited current method (Figure S4). The calculated μ_h and μ_e values are listed in Table 2. The hole mobility of the terpolymer J52-TBF50/ITIC blend film was calculated to be 10.06×10^{-4} cm^2 V^{-1} s^{-1}, which was 1 order of magnitude higher than that of the J52/ITIC blend film and 2-fold higher than that of the TBF100/ITIC blend. The same trend can be detected for electron mobility. The increased and balanced hole/electron mobilities can be attributed to the increased aggregation caused by the increasing content (0−50%) of TBF units in terpolymers, which was confirmed by the GIWAXS measurements and temperature-dependent UV curves. In addition, excessive aggregation of copolymer TBF100 negatively impacted the mobilities in the blend films, which was probably correlated with the variation in the BHJ morphologies. Notably, the incorporation of a rational proportion of TBF units can improve both the hole and electron mobilities, thus promoting charge extraction,[67] which can partly explain the high J_{sc} and FF for J52-TBF50/ITIC-based PSCs.

To better understand the correlation between the proportion of TBF in the terpolymers and the exciton dissociation process, the photocurrent density (J_{ph}) versus the effective voltage (V_{eff}) was measured (Figure 3c). J_{ph} is determined by $J_L - J_D$ (J_L and J_D represent the current density under light and in the dark, respectively), and V_{eff} is obtained from $V_0 - V_a$ (V_0 is the voltage when $J_{ph} = 0$, and V_a is the bias voltage).[68] The J_{ph} was determined to be saturated at $V_{eff} = 4.0$ V for all of the devices, which suggested that the photogenerated excitons were almost entirely dissociated into free charge carriers and collected by the electrodes.[69] The exciton dissociation probability ($P_{diss} = J_{ph}/J_{sat}$) is related to the exciton dissociation and charge collection efficiency, where the J_{sat} value is defined as the saturation photocurrent density. In the short-circuit state, the J52-TBF20-, J52-TBF50-, and J52-TBF80-based devices showed P_{diss} values of 97.0, 96.2, and 95.3%, respectively, which were substantially higher than those of the J52-TBF0-based device (75%) and TBF100-based device (86.7%). These results clearly suggested that more efficient charge dissociation and charge collection processes were achieved when TBF units were randomly incorporated into a BDT-based D−A copolymer, which was consistent with their EQE and J_{sc} values. The degrees of charge recombination were explored by measuring the light intensity (P) dependence

Table 2. Photovoltaic Parameters of the PSCs with Active Areas of 0.1 cm^2 under the Illumination of AM 1.5 G, 100 mW cm^{-2}

polymer	V_{OC}[a] (V)	J_{SC}[a] (mA cm^{-2})	J_{SC}^{EQE}	FF[a]	PCE[a] (%)	μ_h (10^{-4} cm^2 V^{-1} s^{-1})	μ_e (10^{-4} cm^2 V^{-1} s^{-1})
J52-TBF0	0.832 (0.829 ± 0.003)	11.50 (11.28 ± 0.24)	11.44	0.586 (0.578 ± 0.012)	5.61 (5.49 ± 0.12)	1.05 (0.88 ± 0.14)	0.91 (0.73 ± 0.16)
J52-TBF20		17.68 (17.47 ± 0.20)	17.09		10.00 (9.92 ± 0.10)	5.19 (4.63 ± 0.48)	5.68 (5.02 ± 0.59)
J52-TBF50	0.803 (0.801 ± 0.003)	17.93 (17.75 ± 0.13)	17.32	0.705 (0.696 ± 0.008)	10.32 (10.18 ± 0.15)	10.06 (9.27 ± 0.74)	9.33 (8.68 ± 0.60)
J52-TBF80		16.76 (16.48 ± 0.18)	16.38		8.44 (8.30 ± 0.14)	6.49 (5.93 ± 0.52)	5.52 (4.80 ± 0.65)
TBF100	0.790 (0.788 ± 0.004)	15.57 (15.38 ± 0.15)	15.22	0.728 (0.718 ± 0.010)	7.68 (7.52 ± 0.15)	4.92 (4.37 ± 0.51)	5.67 (4.97 ± 0.62)

[a]The values in parentheses are the average values with standard deviations obtained from 15 devices.

DOI: 10.1021/acs.chemmater.9b01957
Chem. Mater. 2019, 31, 6163−6173

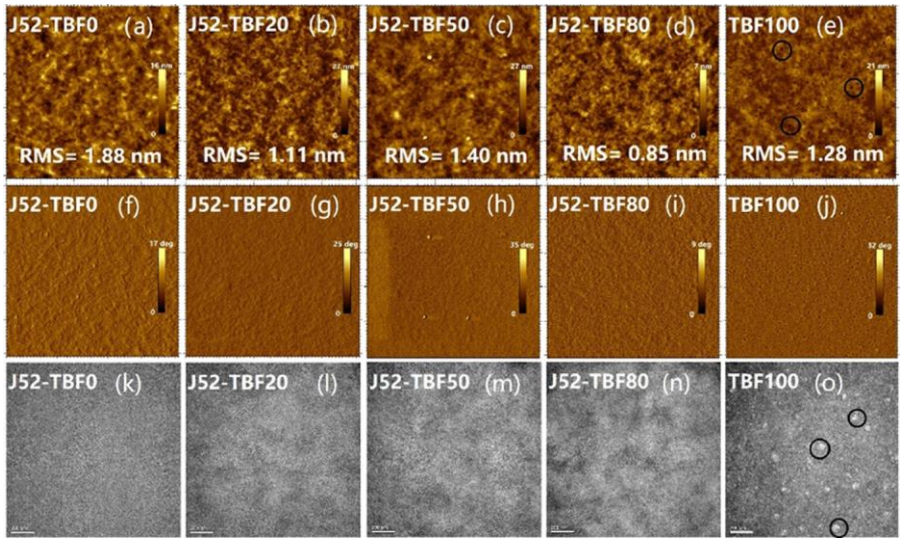

Figure 4. (a−e) Tapping-mode AFM height and (f−j) phase images (5 × 5 μm) for polymer/ITIC blend films with different TBF contents. (k−o) TEM images of polymer/ITIC blend films with different TBF contents.

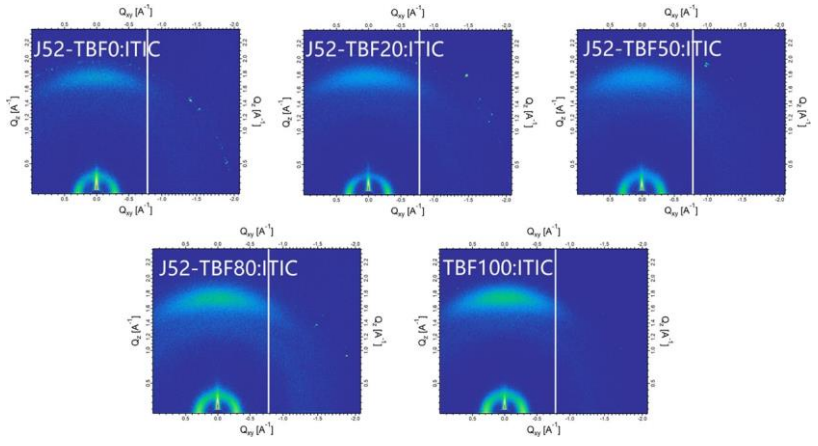

Figure 5. Two-dimensional-GIWAXS patterns of the blend films.

of the $J-V$ curves. J_{sc} followed a power-law dependence on P, and their relationship could be described as $J_{sc} \propto P^S$, where S should be close to 1.0 when the bimolecular recombination is very weak.[70,71] As shown in Figure 3d, the three terpolymers with TBF contents ranging from 20 to 80% showed S values near 0.970, which was much higher than those of D−A copolymers J52-TBF0 (0.892) and TBF100 (0.919), indicating that less biomolecular recombination occurred in the devices based on these random terpolymers. Therefore, integrating BDT and TBF segments into the terpolymer can improve the exciton dissociation probability and reduce bimolecular recombination, ultimately enhancing J_{sc} and FF.

To provide further insight into the variations in exciton transport and separation in the blend films upon incorporation of TBF units into the D−A copolymer backbone, photoluminescence (PL), PL quenching, and transient PL (TPL) spectra were recorded. All of the samples were excited at 520 nm. For the TPL spectroscopy, the emission was probed at a wavelength of 650 nm. Figure 3e shows that the five pure polymer films exhibited strong PL emissions in the range of 600 to 700 nm when excited at 520 nm. The PL spectra were slightly red-shifted as the content of the TBF segment increased. However, the PL emissions were largely quenched in the polymer/ITIC blend films, suggesting efficient electron transfer from the polymer donors to the small molecule acceptors. Notably, the terpolymers possessing both BDT and TBF units exhibited slightly higher quenching efficiencies, which resulted in higher charge transfer in their devices. As shown in Figures 3f and S5, in comparison with the five neat polymer films that present PL lifetimes of around 6 ns, all of the polymer/ITIC films show remarkably shorter PL lifetimes. The fitted lifetimes of J52-TBF0/ITIC, J52-TBF20/ITIC, J52-TBF50/ITIC, J52-TBF80/ITIC, and TBF100/ITIC were obtained to be 1.20, 1.08, 1.01, 1.09, and 1.08 ns, respectively. As the photogenerated exciton is dissociated before luminescence occurs, the shorter decay time implied faster exciton dissociated rate,[72−74] which could be attributed to the appropriate inner bicontinuous network of the blend film, leading to effectively exciton dissociation and charge transfer. Therefore, integrating BDT and TBF segments into the terpolymer at a suitable ratio, such as J52-TBF50, could achieve a higher PCE.

Film Morphology Characterization. To investigate the surface and bulk morphologies of the active layer, we conducted atomic force microscopy (AFM) and transmission electron microscopy (TEM) measurements. The blend films

DOI: 10.1021/acs.chemmater.9b01957
Chem. Mater. 2019, 31, 6163−6173

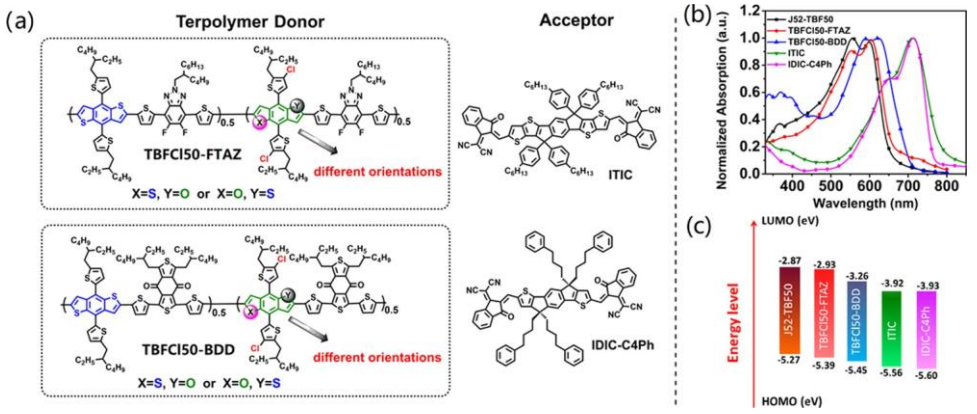

Figure 6. (a) Chemical structures of the target terpolymers and acceptors. (b) UV−vis absorption spectra of the terpolymers and acceptors in solid films. (c) Energy-level diagram of the terpolymers and acceptors.

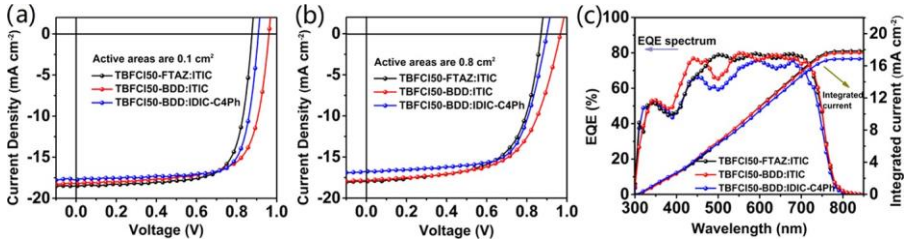

Figure 7. $J-V$ characteristics of the optimized PSCs based on TBFCl50-FTAZ/ITIC, TBFCl50-BDD/ITIC, and TBFCl50-BDD/IDIC-C4Ph with (a) small device areas and (b) large device areas under the illumination of AM 1.5 G, 100 mW cm^{-2}. (c) EQE curves and integrated J_{sc} of the corresponding PSCs with small device areas.

were prepared under the same conditions used for device fabrication. As shown in Figure 4a−e, all of the films were smooth with low root-mean-squared roughness values (∼0.9−1.9 nm). The phase images (Figure 4f−i) revealed that all of the blend films possessed a well-developed fibrillar nanophase with favorable bicontinuous interpenetrating networks. The greatest difference in these blends is that the TBF100/ITIC film showed a large number of nanoscale aggregates, which can be attributed to the strong aggregation of the TBF units (Figure 4e,j). This conspicuous aggregation can also be observed from the TEM image of the TBF100/ITIC blend film (Figure 4o) and is consistent with the results of our previous work.[56] The TEM images (Figure 4k−n) showed that the phase separation gradually became clearer as the content of the TBF segment increased, leading to a great variation in J_{sc} and FF. The GIWAXS patterns of the blend films (Figure 5) showed that the intensity of the (010) π−π stacking peaks along the out-of-plane direction gradually increased with increasing TBF content in the backbone, which is similar to what is seen in the neat polymer films. The high crystallinity of TBF100/ITIC signified excessive aggregation in some areas, as observed from the TEM measurement (Figure 4o), and this aggregation led to an increased probability of exciton recombination. In contrast, J52-TBF20/ITIC and J52-TBF50/ITIC showed moderate crystallinities, which could promote the BHJ and balance the miscibility and ordered packing, resulting in higher J_{sc} and FF values. Overall, the above results confirmed that the proposed terpolymer strategy, combining BDT and TBF segments randomly in the backbone, can be used to adjust the intermolecular aggregation and donor/acceptor miscibility by optimizing the content of TBF moieties.

Molecular Design of High V_{oc} and PCE Terpolymers Integrating BDT and TBF Segments. To confirm the broad utility of our terpolymer strategy, two new BDT-A-TBF-A terpolymers, TBFCl50-FTAZ and TBFCl50-BDD, were synthesized by modifying the side chains of the TBF units with a Cl atom, as shown in Figure 6a. According to recent studies, the insertion of Cl into a conjugated thienyl side chain can decrease the HOMO level because of the electronegativity of Cl.[75,76] On the other hand, chlorination of the conjugated polymers can modulate the molecular interactions and their polarizability, enhancing the crystallinity of the polymer and optimizing the morphology in the BHJ blending.[22,77] The M_n values are listed in Table S1, and the photoelectric properties are shown in Figures 6b,c and S6. As expected, the deeper HOMO levels were measured for TBFCl50-FTAZ and TBFCl50-BDD, indicating that an enhanced V_{oc} and PCE can be anticipated from corresponding terpolymer-based PSCs.

Device Performance and Universality of the Terpol- ymer Strategy. To verify the universality of the terpolymer strategy, two acceptors, ITIC and IDIC-C4Ph, were utilized (see Figure 6a), and PSCs consisting of TBFCl50-FTAZ/ITIC, TBFCl50-BDD/ITIC, and TBFCl50-BDD/IDIC-C4Ph were fabricated in a conventional device configuration of ITO/PEDOT:PSS/active layer/PDINO/Al. The acceptors were selected according to their complementary absorption spectra with the two new terpolymers and their relatively high efficiencies reported in nonfullerene PSCs. The devices were optimized by different conditions (D/A weight ratios, additive, TA, and SVA) with CB as the processing solvent. The best weight ratios for TBFCl50-FTAZ/ITIC, TBFCl50-BDD/ITIC, and TBFCl50-BDD/IDIC-C4Ph were confirmed to be 1:0.8, 1:1.25, and 1:1, respectively. Combination of CB, SVA, and TA treatment at 140 °C for 5 min can slightly improve

DOI: 10.1021/acs.chemmater.9b01957
Chem. Mater. 2019, 31, 6163−6173

Table 3. Photovoltaic Parameters of the PSCs under the Illumination of AM 1.5 G, 100 mW cm^{-2}

blend	active area (cm^2)	V [a] (V)	J [a] (mA cm^{-2})	J_{sc} EQE (mA cm^{-2})	FF[a] (%)	PCE[a] (%)
TBFCl50-FTAZ/ITIC	0.10	0.876 (0.874 ± 0.006)	18.45 (18.20 ± 0.26)	17.85	0.738 (0.728 ± 0.008)	11.94 (11.78 ± 0.12)
TBFCl50-BDD/ITIC	0.10	0.961 (0.958 ± 0.004)	18.17 (17.96 ± 0.14)	17.63	0.713 (0.706 ± 0.009)	12.46 (12.25 ± 0.23)
TBFCl50-BDD/IDIC-C4Ph	0.10	0.908 (0.905 ± 0.004)	17.66 (17.43 ± 0.18)	16.87	0.766 (0.762 ± 0.006)	12.29 (12.16 ± 0.16)
TBFCl50-FTAZ/ITIC	0.80	0.873 (0.870 ± 0.003)	17.94 (17.58 ± 0.27)	17.16	0.640 (0.627 ± 0.016)	10.02 (9.85 ± 0.20)
TBFCl50-BDD/ITIC	0.80	0.964 (0.959 ± 0.006)	17.85 (17.36 ± 0.36)	17.02	0.619 (0.602 ± 0.021)	10.66 (10.38 ± 0.32)
TBFCl50-BDD/IDIC-C4Ph	0.80	0.900 (0.894 ± 0.005)	16.78 (16.46 ± 0.30)	16.18	0.683 (0.667 ± 0.018)	10.31 (10.08 ± 0.25)

[a]The values in parentheses are the average values with standard deviations obtained from 15 devices.

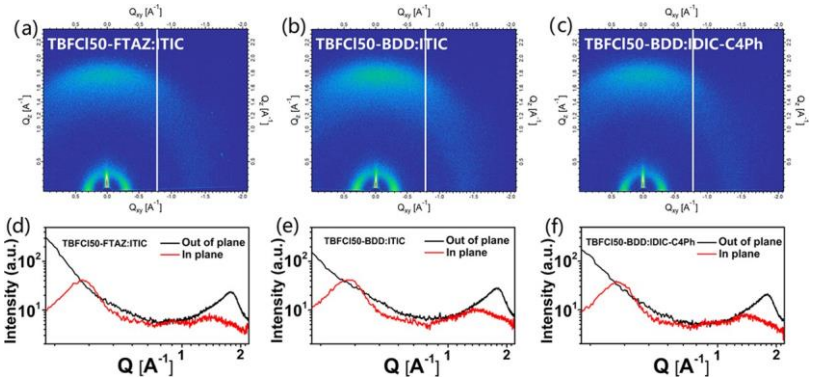

Figure 8. (a−c) Two-dimensional-GIWAXS profiles and (d−f) related in-plane and out-of-plane line-cut profiles of the blend films.

performances for TBFCl50-FTAZ/ITIC- and TBFCl50-BDD/ITIC-based devices. A tiny amount of 1,8-diiodooctane was used to further tune the morphology of the PR2-BDD/ITIC active layer. For the TBFCl50-BDD/IDIC-C4Ph-based device, TA treatment at 90 °C for 10 min resulted in an increase in FF and PCE. As seen from their $J-V$ curves (Figure 7a), EQEs (Figure 7c), and corresponding photovoltaic parameters (Tables 3 and S3 for the performance of all devices tested under different conditions, Supporting Information), the synergetic side chain engineering of the third component, TBF, met the requirements for achieving a high V_{oc} and high performance. Under the optimized conditions, the TBFCl50-FTAZ/ITIC-, TBFCl50-BDD/ITIC-, and TBFCl50-BDD/IDIC-C4Ph-based devices with active areas of 0.1 cm^2 achieved impressive PCEs of 11.94, 12.46, and 12.29%, respectively. Notably, the FFs of these three blend systems were extremely high, especially that of the TBFCl50-BDD/IDIC-C4Ph system, which showed an FF_{max} more than 77% (Table S3), one of the highest values reported for terpolymer-based PSCs to date (Table S4).[10,50] In addition, solar cell devices were fabricated based on different batches of polymers under the same device processing conditions. Small distinctions of photovoltaic performance were observed, which suggests that the molecular weight variations and sequence of BDT and TBF segments in terpolymers are not strongly subject to batch-to-batch variation (Tables S1 and S5). In these new BDT-A-TBF-A terpolymer systems, the decent V_{oc} and high FF and reproducibility make our design strategy more amenable for fabricating high-performance terpolymer solar cells. Moreover, a large-area device (0.8 cm^2) based on TBFCl50-FTAZ/ITIC, TBFCl50-BDD/ITIC, and TBFCl50-BDD/IDIC-C4Ph achieved decent PCEs of more than 10% (Figure 7b), which exemplified the great potential of terpolymers integrating BDT and TBF segments for the manufacture of large-area PSCs with desirable photovoltaic properties for practical applications.

To elucidate the morphology of the active layer, three different D/A blend films were studied by TEM and GIWAXS. As shown in Figure S7, the three different terpolymer/acceptor pairs exhibited uniform fibril-like interpenetrating networks, which could facilitate exciton separation and transport, leading to the decent J_{sc} and FF. The GIWAXS measurements (Figure 8) show that the three blend films display face-on orientations, as evidenced by the appearance of a periodic (010) peak only in the OOP direction. This result indicates that the ordered molecular packing in the BHJ blend films was not disturbed by the random incorporation of BDT and TBF segments into the terpolymer donors. The moderate crystallinity of the blend films based on the BDT-A-TBF-A polymer is desirable for achieving suitable D/A miscibility, efficient charge transport, and weak exciton recombination.

By combining the above morphology analyses and charge dynamics of the pure polymers and BHJ blend films in multiple donor/acceptor systems, we proposed a possible mechanism for the effect of the terpolymer on the blend film properties. The low-crystallinity copolymer donors present weak stacking, which would weaken the charge transport ability, and the excessive D/A miscibility could lead to increased charge recombination during the transport process (Table 2, Figure 3c,d). In contrast, the excessively high crystallinity copolymer donors often show high volume fractions of ordered single-component polymer-rich phases, which cannot be directly linked to the donor/acceptor mixed phase, leading to serious phase separation and increased exciton recombination (Figure 4e,o). Therefore, the BDT-A-TBF-A terpolymer was designed by reasonably balancing the crystallinity to optimize the morphological properties. The TBF units can act as an intermediate fraction to promote the formation of polymer crystallites and balance the miscibility of the donor and acceptor materials with the interconnected mixed phases,

DOI: 10.1021/acs.chemmater.9b01957
Chem. Mater. 2019, 31, 6163−6173

ultimately facilitating charge generation and transport and leading to high photovoltaic performance.

CONCLUSIONS

In summary, we propose an advanced terpolymer design strategy involving the integration of benzodithiophene (BDT) and thieno[2,3-*f*]benzofuran (TBF) segments to construct a series of terpolymers, which provided high-efficiency PSCs when blended with common small molecule acceptors. The key to the strategy is the utilization of TBF segments, which show ordered packing and high crystallinity. Importantly, for the low-crystalline BDT-based D−A copolymer system, incorporating highly crystalline TBF segments can increase the order of the microstructure, maintain the favorable face-on orientation, and reduce the formation of single-component self-aggregates, resulting in a balance between the crystallinity and miscibility behaviors in the BHJ blend films. In the J52/ITIC system, with this terpolymer strategy, the J52-TBF50-based solar cell exhibits a greatly enhanced efficiency of 10.32% when compared to the J52 device (5.61%) and TBF100 device (7.68%). Explorations of different terpolymer/acceptor systems further confirmed that this design strategy is a universal approach for balancing the crystallinity and miscibility of BHJ and achieving outstanding photovoltaic performance. The devices based on TBFCl50-TAZ/ITIC, TBFCl50-BDD/ITIC, and TBFCl50-BDD/IDIC-C4Ph showed impressive PCEs of 11.94, 12.46, and 12.29%, respectively, with high FF and decent V_{oc} values. Notably, the remarkable FF (more than 76%) recorded with the TBFCl50-BDD/IDIC-C4Ph device is among the highest values for terpolymer-based PSCs reported thus far. Furthermore, the excellent processability of terpolymers enables only slight deviations from the optimal BHJ nanomorphology with a 0.8 cm^2 device area, and PCEs of more than 10% were achieved for all three devices. These results demonstrate that the integration of BDT and TBF segments in random terpolymers is a novel and promising approach for designing high-performance terpolymers and manufacturing large-area PSCs with excellent photovoltaic properties for practical applications.

ASSOCIATED CONTENT

Supporting Information

The Supporting Information is available free of charge on the ACS Publications website at DOI: 10.1021/acs.chemmater.9b01957.

Experimental details of device fabrication and characterizations, TGA analysis, electrochemical measurements, and space charge limited current data and structure data from GIWAXS measurements (PDF)

AUTHOR INFORMATION

Corresponding Authors

*E-mail: liyh@qibebt.ac.cn (Y.L.).
*E-mail: zhengn@scut.edu.cn (N.Z.).
*E-mail: baoxc@qibebt.ac.cn (X.B.).
*E-mail: yangrq@qibebt.ac.cn (R.Y.).

ORCID

Bilal Shahid: 0000-0003-1194-7702
Yonghai Li: 0000-0002-5748-0258
Mingliang Sun: 0000-0002-6245-3844
Xichang Bao: 0000-0001-7325-7550
Renqiang Yang: 0000-0001-6794-7416

Author Contributions

All authors have given approval to the final version of the manuscript.

Notes

The authors declare no competing financial interest.

ACKNOWLEDGMENTS

The authors are deeply grateful to the National Natural Science Foundation of China (51773220, 51573205, and 21502205), the Shandong Provincial Natural Science Foundation (ZR2017ZB0314), the Youth Innovation Promotion Association CAS (2016194), DICP & QIBEBT (UN201709 and UN201805), and the Dalian National Laboratory for Clean Energy (DNL) CAS for financial support.

REFERENCES

(1) Huang, Y.; Kramer, E. J.; Heeger, A. J.; Bazan, G. C. Bulk heterojunction solar cells: morphology and performance relationships. *Chem. Rev.* 2014, *114*, 7006−7043.

(2) Espinosa, N.; Hösel, M.; Jørgensen, M.; Krebs, F. C. Large scale deployment of polymer solar cells on land, on sea and in the air. *Energy Environ. Sci.* 2014, *7*, 855−866.

(3) Dennler, G.; Scharber, M. C.; Brabec, C. J. Polymer-Fullerene Bulk-Heterojunction Solar Cells. *Adv. Mater.* 2009, *21*, 1323−1338.

(4) He, Z.; Xiao, B.; Liu, F.; Wu, H.; Yang, Y.; Xiao, S.; Wang, C.; Russell, T. P.; Cao, Y. Single-junction polymer solar cells with high efficiency and photovoltage. *Nat. Photonics* 2015, *9*, 174−179.

(5) Yan, C.; Barlow, S.; Wang, Z.; Yan, H.; Jen, A. K. Y.; Marder, S. R.; Zhan, X. Non-fullerene acceptors for organic solar cells. *Nat. Rev. Mater.* 2018, *3*, No. 18003.

(6) Cheng, P.; Li, G.; Zhan, X.; Yang, Y. Next-generation organic photovoltaics based on non-fullerene acceptors. *Nat. Photonics* 2018, *12*, 131−142.

(7) Xu, X.; Feng, K.; Bi, Z.; Ma, W.; Zhang, G.; Peng, Q. Single-Junction Polymer Solar Cells with 16.35% Effciency Enabled by a Platinum(II) Complexation Strategy. *Adv. Mater.* 2019, *31*, No. 1901872.

(8) Cui, Y.; Yao, H.; Zhang, J.; Zhang, T.; Wang, Y.; Hong, L.; Xian, K.; Xu, B.; Zhang, S.; Peng, J.; Wei, Z.; Gao, F.; Hou, J. Over 16% efficiency organic photovoltaic cells enabled by a chlorinated acceptor with increased open-circuit voltages. *Nat. Commun.* 2019, *10*, No. 2515.

(9) Yuan, J.; Zhang, Y.; Zhou, L.; Zhang, G.; Yip, H.-L.; Lau, T.-K.; Lu, X.; Zhu, C.; Peng, H.; Johnson, P. A.; Leclerc, M.; Cao, Y.; Ulanski, J.; Li, Y.; Zou, Y. Single-Junction Organic Solar Cell with over 15% Efficiency Using Fused-Ring Acceptor with Electron-Deficient Core. *Joule* 2019, *3*, 1140−1151.

(10) Cui, Y.; Yao, H.; Hong, L.; Zhang, T.; Xu, Y.; Xian, K.; Gao, B.; Qin, J.; Zhang, J.; Wei, Z.; Hou, J. Achieving Over 15% Efficiency in Organic Photovoltaic Cells via Copolymer Design. *Adv. Mater.* 2019, *31*, No. 1808356.

(11) Wang, J.; Zhang, J.; Xiao, Y.; Xiao, T.; Zhu, R.; Yan, C.; Fu, Y.; Lu, G.; Lu, X.; Marder, S. R.; Zhan, X. Effect of Isomerization on High-Performance Nonfullerene Electron Acceptors. *J. Am. Chem. Soc.* 2018, *140*, 9140−9147.

(12) Dai, S.; Zhao, F.; Zhang, Q.; Lau, T.; Li, T.; Liu, K.; Ling, Q.; Wang, C.; Lu, X.; You, W.; Zhan, X. Fused Nonacyclic Electron Acceptors for Efficient Polymer Solar Cells. *J. Am. Chem. Soc.* 2017, *139*, 1336−1343.

(13) Lin, Y.; Zhao, F.; He, Q.; Huo, L.; Wu, Y.; Parker, T. C.; Ma, W.; Sun, Y.; Wang, C.; Zhu, D.; Heeger, A. J.; Marder, S. R.; Zhan, X. High-Performance Electron Acceptor with Thienyl Side Chains for Organic Photovoltaics. *J. Am. Chem. Soc.* 2016, *138*, 4955−4961.

(14) Lin, Y.; He, Q.; Zhao, F.; Huo, L.; Mai, J.; Lu, X.; Su, C.; Li, T.; Wang, J.; Zhu, J.; Sun, Y.; Wang, C.; Zhan, X. A Facile Planar Fused-

DOI: 10.1021/acs.chemmater.9b01957
Chem. Mater. 2019, 31, 6163−6173

Ring Electron Acceptor for As-Cast Polymer Solar Cells with 8.71% Efficiency. *J. Am. Chem. Soc.* 2016, *138*, 2973−2976.
(15) Zhan, X.; Tan, Z.; Domercq, B.; An, Z.; Zhang, X.; Barlow, S.; Li, Y.; Zhu, D.; Kippelen, B.; Marder, S. R. A High-Mobility Electron-Transport Polymer with Broad Absorption and Its Use in Field-Effect Transistors and All-Polymer Solar Cells. *J. Am. Chem. Soc.* 2007, *129*, 7246−7247.
(16) Fan, B.; Du, X.; Liu, F.; Zhong, W.; Ying, L.; Xie, R.; Tang, X.; An, K.; Xin, J.; Li, N.; Ma, W.; Brabec, C. J.; Huang, F.; Cao, Y. Fine-tuning of the chemical structure of photoactive materials for highly efficient organic photovoltaics. *Nat. Energy* 2018, *3*, 1051−1058.
(17) Xiao, Z.; Yang, S.; Yang, Z.; Yang, J.; Yip, H.; Zhang, F.; He, F.; Wang, T.; Wang, J.; Yuan, Y.; Yang, H.; Wang, M.; Ding, L. Carbon−Oxygen-Bridged Ladder-Type Building Blocks for Highly Effcient Nonfullerene Acceptors. *Adv. Mater.* 2018, No. 1804790.
(18) Lin, Y.; Wang, J.; Zhang, Z. G.; Bai, H.; Li, Y.; Zhu, D.; Zhan, X. An electron acceptor challenging fullerenes for efficient polymer solar cells. *Adv. Mater.* 2015, *27*, 1170−1174.
(19) Xiao, Z.; Jia, X.; Ding, L. Ternary organic solar cells offer 14% power conversion efficiency. *Sci. Bull.* 2017, *62*, 1562−1564.
(20) Yao, H.; Ye, L.; Hou, J.; Jang, B.; Han, G.; Cui, Y.; Su, G. M.; Wang, C.; Gao, B.; Yu, R.; Zhang, H.; Yi, Y.; Woo, H. Y.; Ade, H.; Hou, J. Achieving Highly Efficient Nonfullerene Organic Solar Cells with Improved Intermolecular Interaction and Open-Circuit Voltage. *Adv. Mater.* 2017, *29*, No. 1700254.
(21) Liu, T.; Luo, Z.; Fan, Q.; Zhang, G.; Zhang, L.; Gao, W.; Guo, X.; Ma, W.; Zhang, M.; Yang, C.; Li, Y.; Yan, H. Use of two structurally similar small molecular acceptors enabling ternary organic solar cells with high efficiencies and fill factors. *Energy Environ. Sci.* 2018, *11*, 3275−3282.
(22) Zhang, H.; Yao, H.; Hou, J.; Zhu, J.; Zhang, J.; Li, W.; Yu, R.; Gao, B.; Zhang, S.; Hou, J. Over 14% Efficiency in Organic Solar Cells Enabled by Chlorinated Nonfullerene Small-Molecule Acceptors. *Adv. Mater.* 2018, *30*, No. 1800613.
(23) Ye, L.; Hu, H.; Ghasemi, M.; Wang, T.; Collins, B. A.; Kim, J. H.; Jiang, K.; Carpenter, J. H.; Li, H.; Li, Z.; McAfee, T.; Zhao, J.; Chen, X.; Lai, J. L. Y.; Ma, T.; Bredas, J. L.; Yan, H.; Ade, H. Quantitative relations between interaction parameter, miscibility and function in organic solar cells. Ade. *Nat. Mater.* 2018, *17*, 253−260.
(24) Li, G.; Zhu, R.; Yang, Y. Polymer solar cells. *Nat. Photonics* 2012, *6*, 153−161.
(25) Wang, X.; Du, Z.; Dou, K.; Jiang, H.; Gao, C.; Han, L.; Yang, R. A Maverick Asymmetrical Backbone with Distinct Flanked Twist Angles Modulating the Molecular Aggregation and Crystallinity for High Performance Nonfullerene Solar Cells. *Adv. Energy Mater.* 2019, *9*, No. 1802530.
(26) Huang, F.; Wu, H.; Cao, Y. Water/alcohol soluble conjugated polymers as highly efficient electron transporting/injection layer in optoelectronic devices. *Chem. Soc. Rev.* 2010, *39*, 2500−2521.
(27) You, J.; Dou, L.; Yoshimura, K.; Kato, T.; Ohya, K.; Moriarty, T.; Emery, K.; Chen, C. C.; Gao, J.; Li, G.; Yang, Y. A polymer tandem solar cell with 10.6% power conversion efficiency. *Nat. Commun.* 2013, *4*, No. 1446.
(28) Zhang, Z.-G.; Qi, B.; Jin, Z.; Chi, D.; Qi, Z.; Li, Y.; Wang, J. Perylene diimides: a thickness-insensitive cathode interlayer for high performance polymer solar cells. *Energy Environ. Sci.* 2014, *7*, 1966−1973.
(29) Dang, D.; Yu, D.; Wang, E. Conjugated Donor-Acceptor Terpolymers Toward High-Efficiency Polymer Solar Cells. *Adv. Mater.* 2019, *31*, No. 1807019.
(30) Li, J.; Liang, Z.; Wang, Y.; Li, H.; Tong, J.; Bao, X.; Xia, Y. Enhanced Efficiency of Polymer Solar Cells Through Synergistic Optimization of Mobility and Tuning donor Alloys by Adding High-Mobility Conjugated Polymers. *J. Mater. Chem. C* 2018, *6*, 11015.
(31) Li, J.; Wang, Y.; Liang, Z.; Wang, N.; Tong, J.; Yang, C.; Bao, X.; Xia, Y. Enhanced Organic Photovoltaic Performance through Modulating Vertical Composition Distribution and Promoting Crystallinity of the Photoactive Layer by Diphenyl Sulfide Additives. *ACS Appl. Mater. Interfaces* 2019, *11*, 7022−7029.
(32) Lu, L.; Zheng, T.; Wu, Q.; Schneider, A. M.; Zhao, D.; Yu, L. Recent Advances in Bulk Heterojunction Polymer Solar Cells. *Chem. Rev.* 2015, *115*, 12666−12731.
(33) Heeger, A. J. 25th anniversary article: Bulk heterojunction solar cells: understanding the mechanism of operation. *Adv. Mater.* 2014, *26*, 10−27.
(34) Cui, C.; Wong, W.-Y.; Li, Y. Improvement of open-circuit voltage and photovoltaic properties of 2D-conjugated polymers by alkylthio substitution. *Energy Environ. Sci.* 2014, *7*, 2276−2284.
(35) Li, S.; Ye, L.; Zhao, W.; Yan, H.; Yang, B.; Liu, D.; Li, W.; Ade, H.; Hou, J. A Wide Band Gap Polymer with a Deep Highest Occupied Molecular Orbital Level Enables 14.2% Efficiency in Polymer Solar Cells. *J. Am. Chem. Soc.* 2018, *140*, 7159−7167.
(36) Xu, X.; Yu, T.; Bi, Z.; Ma, W.; Li, Y.; Peng, Q. Realizing Over 13% Efficiency in Green-Solvent-Processed Nonfullerene Organic Solar Cells Enabled by 1,3,4-Thiadiazole-Based Wide-Bandgap Copolymers. *Adv. Mater.* 2018, *30*, No. 1703973.
(37) Zhang, M.; Guo, X.; Ma, W.; Ade, H.; Hou, J. A Large-Bandgap Conjugated Polymer for Versatile Photovoltaic Applications with High Performance. *Adv. Mater.* 2015, *27*, 4655−4660.
(38) Duan, C.; Gao, K.; van Franeker, J. J.; Liu, F.; Wienk, M. M.; Janssen, R. A. Toward Practical Useful Polymers for Highly Efficient Solar Cells via a Random Copolymer Approach. *J. Am. Chem. Soc.* 2016, *138*, 10782−10785.
(39) Ye, L.; Jiao, X.; Zhang, S.; Yao, H.; Qin, Y.; Ade, H.; Hou, J. Control of Mesoscale Morphology and Photovoltaic Performance in Diketopyrrolopyrrole-Based Small Band Gap Terpolymers. *Adv. Energy Mater.* 2017, *7*, No. 1601138.
(40) Shin, I.; Ahn, H. j.; Yun, J. H.; Jo, J. W.; Park, S.; Joe, S.-y.; Bang, J.; Son, H. J. High-Performance and Uniform 1 cm^2 Polymer Solar Cells with D1-A-D2-A-Type Random Terpolymers. *Adv. Energy Mater.* 2018, *8*, No. 1701405.
(41) Wang, Q.; Wang, Y.; Zheng, W.; Shahid, B.; Qiu, M.; Wang, D.; Zhu, D.; Yang, R. Regulating Molecular Aggregations of Polymers via Ternary Copolymerization Strategy for Efficient Solar Cells. *ACS Appl. Mater. Interfaces* 2017, *9*, 32126−32134.
(42) Cho, H. J.; Kim, Y. J.; Chen, S.; Lee, J.; Shin, T. J.; Park, C. E.; Yang, C. Over 10% efficiency in single-junction polymer solar cells developed from easily accessible random terpolymers. *Nano Energy* 2017, *39*, 229−327.
(43) Li, Z.; Xu, X.; Zhang, W.; Meng, X.; Ma, W.; Yartsev, A.; Inganas, O.; Andersson, M. R.; Janssen, R. A.; Wang, E. High Performance All-Polymer Solar Cells by Synergistic Effects of Fine-Tuned Crystallinity and Solvent Annealing. *J. Am. Chem. Soc.* 2016, *138*, 10935−10944.
(44) Kelly, M. A.; Zhang, Q.; Peng, Z.; Noman, V.; Zhu, C.; Ade, H.; You, W. The finale of a trilogy: comparing terpolymers and ternary blends with structurally similar backbones for use in organic bulk heterojunction solar cells. *J. Mater. Chem. A* 2018, *6*, 19190−19200.
(45) Qu, S.; Wang, H.; Mo, D.; Chao, P.; Yang, Z.; Li, L.; Tian, L.; Chen, W.; He, F. Fine Tuning of Open-Circuit Voltage by Chlorination in Thieno[3,4-b]thiophene−Benzodithiophene Terpolymers toward Enhanced Solar Energy Conversion. *Macromolecules* 2017, *50*, 4962−4971.
(46) Li, Z.; Weng, K.; Chen, A.; Sun, X.; Wei, D.; Yu, M.; Huo, L.; Sun, Y. Benzothiadiazole Versus Thiophene: Influence of the Auxiliary Acceptor on the Photovoltaic Properties of Donor-Acceptor-Based Copolymers. *Macromol. Rapid Commun.* 2018, *39*, No. 1700547.
(47) Li, K.; Hu, Z.; Zeng, Z.; Huang, Z.; Zhong, W.; Ying, L.; Huang, F.; Cao, Y. Improved performance of non-fullerene polymer solar cells using wide-bandgap random terpolymers. *Org. Electron.* 2018, *57*, 317−322.
(48) Kang, T. E.; Kim, K.-H.; Kim, B. J. Design of terpolymers as electron donors for highly efficient polymer solar cells. *J. Mater. Chem. A* 2014, *2*, 15252−15267.
(49) Jeong, M.; Chen, S.; Lee, S. M.; Wang, Z.; Yang, Y.; Zhang, Z.; Zhang, C.; Xiao, M.; Li, Y.; Yang, C. Feasible D1−A−D2−A Random Copolymers for Simultaneous High-Performance Fullerene. *Adv. Energy Mater.* 2018, *8*, No. 1702166.

DOI: 10.1021/acs.chemmater.9b01957
Chem. Mater. 2019, 31, 6163−6173

(50) Xie, Q.; Liao, X.; Chen, L.; Zhang, M.; Gao, K.; Huang, B.; Xu, H.; Liu, F.; Jen, A. K.; Chen, Y. Random copolymerization realized high efficient polymer solar cells with a record fill factor near 80%. *Nano Energy* 2019, *61*, 228−235.
(51) Chen, S.; Cho, H. J.; Lee, J.; Yang, Y.; Zhang, Z.; Li, Y.; Yang, C. Modulating the Molecular Packing and Nanophase Blending via a Random Terpolymerization Strategy toward 11% Effciency Non-fullerene Polymer Solar Cells. *Adv. Energy Mater.* 2017, *7*, No. 1701125.
(52) Deng, P.; Wu, B.; Lei, Y.; Cao, H.; Ong, B. S. Regioregular and Random Difluorobenzothiadiazole Electron Donor−Acceptor Polymer Semiconductors for Thin-Film Transistors and Polymer Solar Cells. *Macromolecules* 2016, *49*, 2541−2548.
(53) Liao, X.; Zhang, L.; Chen, L.; Hu, X.; Ai, Q.; Ma, W.; Chen, Y. Room temperature processed polymers for high-efficient polymer solar cells with power conversion efficiency over 9%. *Nano Energy* 2017, *37*, 32−39.
(54) Kim, K.-H.; Park, S.; Yu, H.; Kang, H.; Song, I.; Oh, J. H.; Kim, B. J. Determining Optimal Crystallinity of Diketopyrrolopyrrole-Based Terpolymers for Highly Efficient Polymer Solar Cells and Transistors. *Chem. Mater.* 2014, *26*, 6963−6970.
(55) Hwang, Y. J.; Earmme, T.; Courtright, B. A.; Eberle, F. N.; Jenekhe, S. A. n-Type semiconducting naphthalene diimide-perylene diimide copolymers: controlling crystallinity, blend morphology, and compatibility toward high-performance all-polymer solar cells. *J. Am. Chem. Soc.* 2015, *137*, 4424−4434.
(56) Dou, K.; Wang, X.; Du, Z.; Jiang, H.; Li, F.; Sun, M.; Yang, R. Synergistic effect of side-chain and backbone engineering in thieno[2,3-f]benzofuran-based conjugated polymers for high performance non-fullerene organic solar cells. *J. Mater. Chem. A* 2019, *7*, 958−964.
(57) Gao, Y.; Zhu, R.; Wang, Z.; Guo, F.; Wei, Z.; Yang, Y.; Zhao, L.; Zhang, Y. An Asymmetrical Polymer Based on Thieno[2,3-f]benzofuran for Efficient Fullerene-Free Polymer Solar Cells. *ACS Appl. Energy Mater.* 2018, *1*, 1888−1892.
(58) Bin, H.; Zhang, Z. G.; Gao, L.; Chen, S.; Zhong, L.; Xue, L.; Yang, C.; Li, Y. Non-Fullerene Polymer Solar Cells Based on Alkylthio and Fluorine Substituted 2D-Conjugated Polymers Reach 9.5% Efficiency. *J. Am. Chem. Soc.* 2016, *138*, 4657−4664.
(59) Bin, H.; Gao, L.; Zhang, Z. G.; Yang, Y.; Zhang, Y.; Zhang, C.; Chen, S.; Xue, L.; Yang, C.; Xiao, M.; Li, Y. 11.4% Efficiency non-fullerene polymer solar cells with trialkylsilyl substituted 2D-conjugated polymer as donor. *Nat. Commun.* 2016, *7*, No. 13651.
(60) Liao, Z.; Xie, Y.; Chen, L.; Tan, Y.; Huang, S.; An, Y.; Ryu, H. S.; Meng, X.; Liao, X.; Huang, B.; Xie, Q.; Woo, H. Y.; Sun, Y.; Chen, Y. Fluorobenzotriazole (FTAZ)-Based Polymer Donor Enables Organic Solar Cells Exceeding 12% Efficiency. *Adv. Funct. Mater.* 2019, No. 1808828.
(61) He, D.; Zhao, F.; Xin, J.; Rech, J. J.; Wei, Z.; Ma, W.; You, W.; Li, B.; Jiang, L.; Li, Y.; Wang, C. A Fused Ring Electron Acceptor with Decacyclic Core Enables over 13.5% Efficiency for Organic Solar Cells. *Adv. Energy Mater.* 2018, *8*, No. 1802050.
(62) Zhang, J.; Liu, W.; Chen, S.; Xu, S.; Yang, C.; Zhu, X. One-pot synthesis of electron-acceptor composite enables efficient fullerene-free ternary organic solar cells. *J. Mater. Chem. A* 2018, *6*, 22519−22525.
(63) Li, Y.; Zheng, N.; Yu, L.; Wen, S.; Gao, C.; Sun, M.; Yang, R. A Simple Phenyl Group Introduced at the Tail of Alkyl Side Chains of Small Molecular Acceptors: New Strategy to Balance the Crystallinity of Acceptors and Miscibility of Bulk Heterojunction Enabling Highly Efficient Organic Solar Cells. *Adv. Mater.* 2019, *31*, No. 1807832.
(64) Li, Z.; Jiang, K.; Yang, G.; Lai, J. Y. L.; Ma, T.; Zhao, J.; Ma, Wei.; Yan, H. Donor polymer design enables efficient non-fullerene organic solar cells. *Nat. Commun.* 2016, *7*, No. 13094.
(65) Xue, X.; Weng, K.; Qi, F.; Zhang, Y.; Wang, Z.; Ali, J.; Wei, D.; Sun, Y.; Liu, F.; Wan, M.; Liu, J.; Huo, L. Steric engineering of alkylthiolation side chains to finely tune miscibility in nonfullerene polymer solar cells. *Adv. Energy Mater.* 2019, *9*, No. 1802686.
(66) Cardona, C. M.; Li, W.; Kaifer, A. E.; Stockdale, D.; Bazan, G. C. Electrochemical considerations for determining absolute frontier orbital energy levels of conjugated polymers for solar cell applications. *Adv. Mater.* 2011, *23*, 2367−2371.
(67) Liu, D.; Wang, J.; Gu, C.; Li, Y.; Bao, X.; Yang, R. Stirring Up Acceptor Phase and Controlling Morphology via Choosing Appropriate Rigid Aryl Rings as Lever Arms in Symmetry-Breaking Benzodithiophene for High-Performance Fullerene and Fullerene-Free Polymer Solar Cells. *Adv. Mater.* 2018, *30*, No. 1705870.
(68) Wu, J.-L.; Chen, F.; Hsiao, Y.; Chien, F.; Chen, P.; Kuo, C.; Huang, M. H.; Hsu, C. Surface Plasmonic Effects of Metallic Nanoparticles on the Performance of Polymer Bulk Heterojunction Solar Cells. *ACS Nano* 2011, *5*, 959−967.
(69) Mihailetchi, V. D.; Koster, L. J.; Hummelen, J. C.; Blom, P. W. Photocurrent generation in polymer-fullerene bulk heterojunctions. *Phys. Rev. Lett.* 2004, *93*, 216601−216604.
(70) Schilinsky, P.; Waldauf, C.; Brabec, C. J. Recombination and loss analysis in polythiophene based bulk heterojunction photodetectors. *Appl. Phys. Lett.* 2002, *81*, 3885−3887.
(71) Cowan, S. R.; Roy, A.; Heeger, A. J. Recombination in polymer-fullerene bulk heterojunction solar cells. *Phys. Rev. B* 2010, *82*, No. 245207.
(72) Huang, J.-S.; Goh, T.; Li, X.; Sfeir, M. Y.; Bielinski, E. A.; Tomasulo, S.; Lee, M. L.; Hazari, N.; Taylor, A. D. Polymer bulk heterojunction solar cells employing Förster resonance energy transfer. *Nat. Photonics* 2013, *7*, 479−485.
(73) Liang, Z.; Tong, J.; Li, H.; Wang, Y.; Wang, N.; Li, J.; Yang, C.; Xia, Y. The comprehensive utilization of the synergistic effect of fullerene and non-fullerene acceptors to achieve highly efficient polymer solar cells. *J. Mater. Chem. A* 2019, *7*, 15841−15850.
(74) Chen, X.; Tao, S.; Fan, C.; Chen, D.; Zhou, L.; Lin, H.; Zheng, C.; Su, S. Ternary Organic Solar Cells with Coumarin7 as the Donor Exhibiting Greater Than 10% Power Conversion Efficiency and a High Fill Factor of 75%. *ACS Appl. Mater. Interfaces* 2017, *9*, 29907−29916.
(75) Wang, H.; Chao, P.; Chen, H.; Mu, Z.; Chen, W.; He, F. Simultaneous Increase in Open-Circuit Voltage and Efficiency of Fullerene-Free Solar Cells through Chlorinated Thieno[3,4-b]-thiophene Polymer Donor. *ACS Energy Lett.* 2017, *2*, 1971−1977.
(76) Zhang, Y.; Gao, X.; Li, J.; Tu, G. Highly selective palladium-catalyzed Stille coupling reaction toward chlorine-containing NIR electroluminescent polymers. *J. Mater. Chem. C* 2015, *3*, 7463−7468.
(77) Liu, Z.; Gao, Y.; Dong, J.; Yang, M.; Liu, M.; Wen, J.; Zhang, Y.; Ma, H.; Gao, X.; Chen, W.; Shao, M. Chlorinated Wide Bandgap Donor Polymer Enabling Annealing Free Non-Fullerene Solar Cells with the Efficiency of 11.5%. *J. Phys. Chem. Lett.* 2018, *9*, 6955−6962.

DOI: 10.1021/acs.chemmater.9b01957
Chem. Mater. 2019, 31, 6163−6173